Volume 14
Number 14
14 April 2022
Pages 5251-5628

Nanoscale

rsc.li/nanoscale

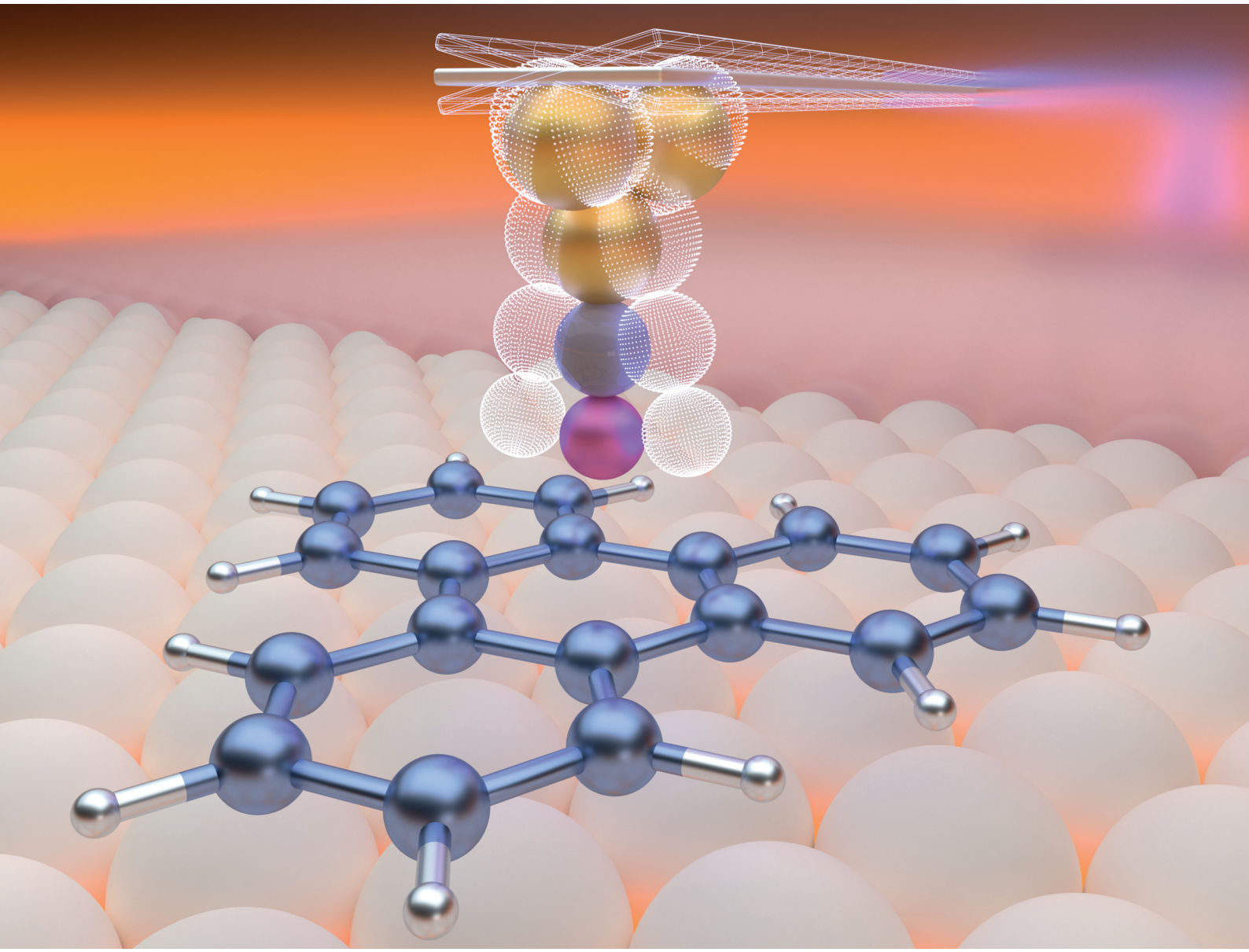

ISSN 2040-3372

ROYAL SOCIETY OF CHEMISTRY

PAPER
Daniel Ebeling *et al.*
Chemical bond imaging using torsional and flexural higher eigenmodes of qPlus sensors

NCNST

Nanoscale

PAPER

View Article Online
View Journal | View Issue

Cite this: *Nanoscale*, 2022, **14**, 5329

Chemical bond imaging using torsional and flexural higher eigenmodes of qPlus sensors†

Daniel Martin-Jimenez, [a,b] Michael G. Ruppert, [c] Alexander Ihle, [a,b] Sebastian Ahles, [d,b] Hermann A. Wegner, [d,b] André Schirmeisen [a,b] and Daniel Ebeling *[a,b]

Received 23rd February 2022,
Accepted 21st March 2022

DOI: 10.1039/d2nr01062c

rsc.li/nanoscale

Non-contact atomic force microscopy (AFM) with CO-functionalized tips allows visualization of the chemical structure of adsorbed molecules and identify individual inter- and intramolecular bonds. This technique enables in-depth studies of on-surface reactions and self-assembly processes. Herein, we analyze the suitability of qPlus sensors, which are commonly used for such studies, for the application of modern multifrequency AFM techniques. Two different qPlus sensors were tested for submolecular resolution imaging *via* actuating torsional and flexural higher eigenmodes and *via* bimodal AFM. The torsional eigenmode of one of our sensors is perfectly suited for performing lateral force microscopy (LFM) with single bond resolution. The obtained LFM images agree well with images from the literature, which were scanned with customized qPlus sensors that were specifically designed for LFM. The advantage of using a torsional eigenmode is that the same molecule can be imaged either with a vertically or laterally oscillating tip without replacing the sensor simply by actuating a different eigenmode. Submolecular resolution is also achieved by actuating the 2nd flexural eigenmode of our second sensor. In this case, we observe particular contrast features that only appear in the AFM images of the 2nd flexural eigenmode but not for the fundamental eigenmode. With complementary laser Doppler vibrometry measurements and AFM simulations we can rationalize that these contrast features are caused by a diagonal (*i.e.* in-phase vertical and lateral) oscillation of the AFM tip.

1. Introduction

Since its invention in 1986,[1] atomic force microscopy (AFM) has experienced great progress by enhancing the resolution and performance for surface characterization.[2–6] One of the most recent developments is the so-called "bond imaging AFM technique", which allows the visualization of individual organic compounds with submolecular resolution.[7] With this method, sequential chemical reaction steps can, for example, be followed with single bond resolution.[8–19] Therefore, the bond imaging technique became an inevitable tool for deciphering the mechanisms of on-surface synthesis.[20,21]

Experimentally, submolecular resolution is commonly achieved by utilizing qPlus sensors[22] with CO-functionalized tips[23,24] that are mechanically actuated close to their fundamental resonance (f_1) in ultra-high vacuum conditions at low temperature ($p < 10^{-10}$ mbar, T ≈ 5.2 K). The images are usually obtained in constant-height or constant-current mode[25] by tracking changes in the fundamental frequency of the sensor[26] that are caused by short range interactions between the CO tip and the atoms of the imaged molecule. The qPlus type sensors are nowadays used in most commercial low temperature AFM systems since no laser is required for the signal read out and they have proven their high-resolution capabilities.[27] In contrast to conventional silicon cantilevers the spring constants of qPlus sensors are relatively high (1800 N m^{-1}) and relatively small oscillation amplitudes on the order of 50 pm are accessible.

In case of conventional silicon cantilevers the simultaneous actuation of their fundamental and higher flexural or torsional eigenmodes can offer, for example, more channels of information, higher image contrast or increased force sensitivity.[28–47] The suitability of qPlus sensors for the application of such modern multifrequency operation modes has, however, only been scarcely studied until now.[48–54] For

[a]*Institute of Applied Physics (IAP), Justus Liebig University Giessen, Heinrich-Buff-Ring 16, Giessen 35392, Germany. E-mail: Daniel.Ebeling@ap.physik.uni-giessen.de*
[b]*Center for Materials Research (LaMa), Justus Liebig University Giessen, Heinrich-Buff-Ring 16, Giessen 35392, Germany*
[c]*University of Newcastle, Callaghan, NSW 2308, Australia*
[d]*Institute of Organic Chemistry, Justus Liebig University Giessen, Heinrich-Buff-Ring 17, Giessen 35392, Germany*

†Electronic supplementary information (ESI) available: Fig. S1–S4. See DOI: https://doi.org/10.1039/d2nr01062c

example, it has been observed that flat crystalline NaCl and KBr surfaces can be imaged with atomic resolution using a higher eigenmode or bimodal AFM in UHV and ambient conditions.[48,50,53] It has also been reported that higher eigenmodes can lead to lateral movements of the tip that could be useful for dynamic lateral force microscopy (LFM).[53] Recently, we demonstrated that higher eigenmodes of qPlus sensors allow bond imaging of individual organic compounds.[51]

Here, we systematically analyze the bond imaging contrast that can be obtained by actuating higher torsional and flexural eigenmodes of qPlus sensors and by using bimodal AFM. Two different qPlus sensors with slightly different fundamental resonance frequencies of 25.87 kHz and 26.97 kHz, respectively, were used. While sensor 1 only offered submolecular resolution at a torsional eigenmode at 118.44 kHz, sensor 2 only offered submolecular resolution at the 2nd flexural eigenmode at 163.96 kHz. In both cases, the imaging performance was analyzed for different oscillation amplitudes and average tip–substrate distances. The torsional eigenmode of sensor 1 is ideally suited for performing dynamic LFM. It delivers high-quality submolecular resolution images that are in good agreement with the results obtained with special qPlus sensors designed for LFM (sensor and tip rotated by 90°).[55,56] Here, the advantage is that one can easily switch between conventional bond imaging and lateral bond imaging by using either the fundamental or the torsional eigenmode of the same qPlus sensor without changing the sensor. In case of sensor 2, we observe that the image contrast of the 2nd flexural eigenmode is affected by lateral tip oscillations. These image artifacts are discussed in the context of complementary laser Doppler vibrometry measurements, which reveal that the tip oscillations of qPlus sensors possess vertical and lateral components at the 2nd flexural eigenmode.[57] This is underpinned by AFM simulations with the so-called probe particle model.[58]

2. Materials and methods

2.1 Atomic force microscope

AFM images in this article were taken with a commercial LT-AFM/STM (Scienta Omicron, Germany) at a pressure below 10^{-10} mbar and a temperature of about 5.2 K. An external lock-in amplifier electronics (MFLI, Zürich Instruments, Switzerland) was connected to the AFM to operate the qPlus sensor in FM and AM mode. For the detection of torsional and 2nd eigenmode resonances, the qPlus sensors were mechanically actuated with frequencies ranging from 105 kHz to 195 kHz inside the LT-AFM. Fig. S1† shows the spectra of both sensors. Their frequency responses at high frequencies can be rather complex and may contain several peaks. Only at frequencies of 118.44 kHz for sensor 1 and 163.96 kHz for sensor 2 imaging of organic compounds with submolecular resolution was possible. For FM mode, the phase-locked loop was set to give an effective bandwidth of the frequency shift channel of 10 Hz. The AM mode was operated with a bandwidth of the amplitude and phase channel of 10 Hz. All images in this article correspond to raw data that were captured with the mentioned bandwidth and scan speed given in the figure's captions. Only in Fig. 4g the noise was removed using a 2D FFT filter (see details in Fig. S3†). The vertical amplitudes of the flexural eigenmodes were calibrated by applying the method described in Simon *et al.*[59]

2.2 Sample and tip preparation

Molecules imaged in this article were prepared from 2-iodotriphenylene (ITP) as a precursor deposited onto Ag(111) and Cu(111) substrates (Mateck GmbH, Germany). The synthesis of ITP is described in Ref. 25. Ag(111) and Cu(111) were cleaned by multiple Ar^+ sputtering cycles (E = 1.5 kV, I = 2.5–3 μA, p = 6 × 10^{-6} mbar) and annealing cycles with T = 900 K for Ag(111) and T = 1000 K for Cu(111). ITP molecules were deposited onto the precooled substrates (T below 30 K) using a home-built evaporator.[60] Triphenylene (TP) was found as a product after one hour annealing of ITP on Ag(111) at T = 116.8 K. Bistriphenylene (Bis-TP) was detected after one hour annealing of ITP on Ag(111) at room temperature. ITP on Cu(111) were directly imaged after molecule deposition.

The tungsten tip of the qPlus sensors were sharpened in the LT-AFM/STM by voltage pulses and indentations into the sample substrate. For tip functionalization CO was dosed onto the Ag(111) and Cu(111) surfaces. For Ag(111) the tip was functionalized by applying voltage pulses of −1 V for 500 μs above the adsorbed CO molecules, while for Cu(111) the CO-tip was achieved by applying the procedure described in Bartels *et al.*[23]

2.3 Analysis of laser Doppler vibrometer data

Frequency responses of the qPlus sensors were taken by a laser Doppler vibrometer (MSA-100-3D, Polytec). The qPlus sensors were electrically actuated using periodic chirp signal.[57,61] The laser was moved across the top and lateral sides of the free prong. Frequency spectra from 15 kHz to 200 kHz were extracted from different positions on the prong. The mode shapes of the free prong were extracted from the Polytec software by evaluating magnitude and phase of the frequency spectra for each point at selected frequencies.

3. Results and discussion

3.1 Torsional eigenmode

Fig. 1a–d shows constant height frequency shift (Δf) AFM images of triphenylene (TP) on Ag(111) taken with sensor 1 at the torsional eigenmode (f_T = 118.44 kHz) with four different oscillation amplitudes of 28, 56, 112 and 224 pm, respectively. The qPlus sensor was operated in the frequency modulation mode (FM-mode).[26] The image in Fig. 1a was taken with an amplitude of 28 pm and clearly reveals the chemical structure of the TP molecule (see structure in Fig. 1d), *i.e.* the C–C bonds of the molecular backbone appear as dark lines in the frequency shift image. The darkest bonds (see blue arrows in Fig. 1a) are perpendicular to the lateral tip oscillation, which is in good agreement with LFM bond images reported in the literature.[55]

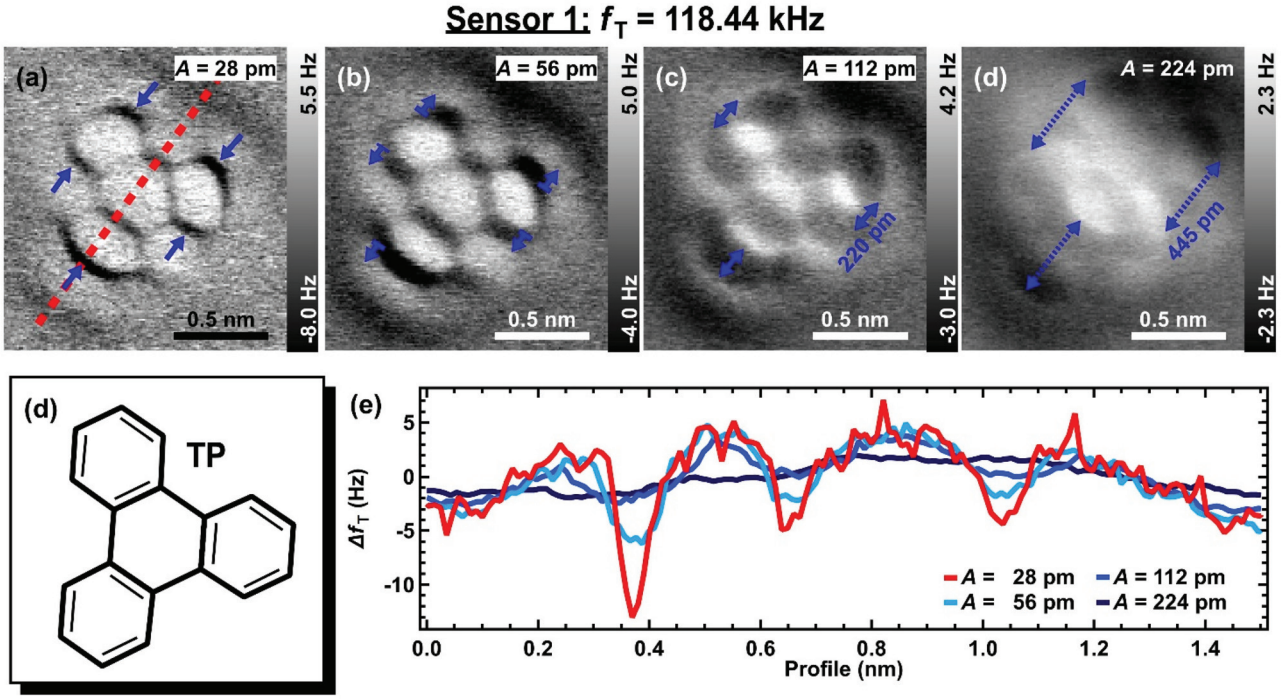

Fig. 1 (a–d) Frequency shift images of TP on Ag(111) at constant height by using sensor 1, which is operated in FM mode at the torsional eigenmode with f_T = 118.44 kHz and oscillation amplitudes of (a) 28 pm, (b) 56 pm, (c) 112 pm and (d) 224 pm. Scan speed: 625 pm s^{-1}. (d) Chemical structure of TP. (e) Profiles along the TP molecule (dashed red line in panel a) for the AFM images a-d.

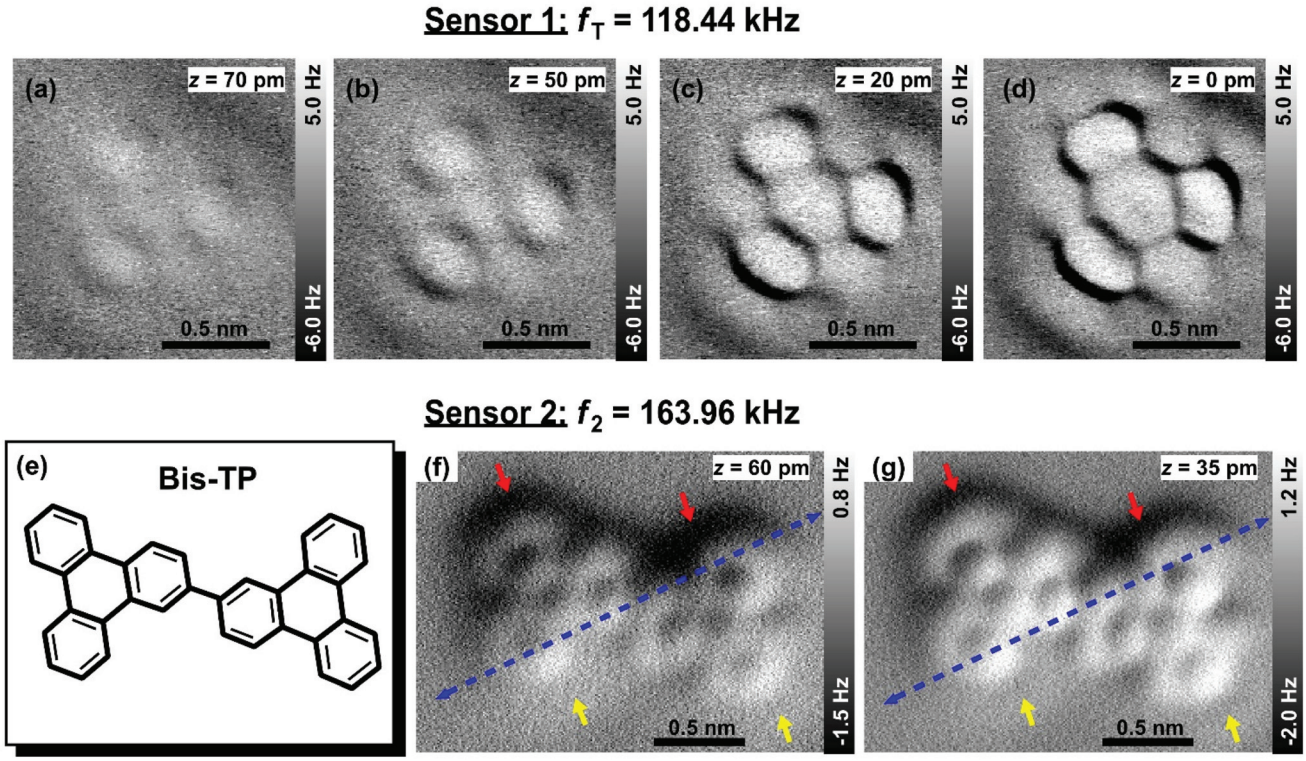

Fig. 2 (a–d) Frequency shift images of TP on Ag(111) at tip–sample separations of (a) 70 pm, (b) 50 pm, (c) 20 pm and (d) 0 pm. Images were taken with sensor 1 in FM mode with f_T = 118.46 kHz and lateral tip amplitudes of 28 pm. Scan speed: 250 pm s^{-1}. Reference for z = 0 pm: I = 20 pA U = 7 mV on Ag(111). (e) Chemical structure of Bis-TP. (f–g) Frequency shift image of Bis-TP deposited on Ag(111) at constant height of (f) 60 pm and (g) 35 pm by using sensor 2 in FM mode with f_2 = 163.96 kHz and a flexural amplitudes of 21 pm. Scan speed: 500 pm s^{-1}. Reference for z = 0 pm: I = 20 pA U = 7 mV on Ag(111).

By increasing the amplitude, the features perpendicular to the tip oscillation become wider (see blue arrows in Fig. 1b–d), which also agrees well with previous LFM results.[55] At lateral oscillation amplitudes of 112 pm and 224 pm, the widening is on the order of 220 pm and 445 pm, respectively, which makes it difficult to identify the molecular structures (Fig. 1c and 1d).

In Fig. 1e, corresponding single line profiles of the images in Fig. 1a–d are depicted. The path of the line profiles is exemplarily indicated in Fig. 1a by the dashed red line. These profiles also reveal widening of image features with increasing lateral oscillation amplitudes. This agrees well with previous findings for customized LFM sensors.[55] The length of the blue arrows in Fig. 1c and 1d was correlated to the peak-to-peak amplitude of the lateral tip oscillation, revealing a sensitivity of the torsional eigenmode of 1.12 pm μV^{-1}.[62]

Fig. 2 shows LFM images that were obtained with sensor 1 at the torsional eigenmode and with a lateral oscillation amplitude of 28 pm for four different average tip–substrate distances. The dependence of the LFM contrast on the average tip–substrate distance[56] is rather strong as illustrated by the images in Fig. 2a–d, which use the same contrast scaling. This also indicates that the tip oscillates predominantly in the lateral direction.

3.2 Second flexural eigenmode

Sensor 1 did not offer a good frequency shift response at any of the spectral peaks with frequencies around 6.3 times f_1[33,52] (see amplitude *vs.* drive frequency spectra for the sensors 1 and 2 in Fig. S1†). Therefore, it was not possible to perform bond imaging experiments at the 2nd flexural eigenmode of sensor 1. By contrast, sensor 2 did offer an excellent peak in the spectrum at 163.96 kHz with a Q-factor of $Q \approx 30\,000$ (Fig. S1b†). Operating sensor 2 at this peak, enabled imaging of bistriphenylene (Bis-TP, see structure in Fig. 2e) on Ag(111) in constant-height mode. Fig. 2f–g displays images of Bis-TP with an oscillation amplitude of 21 pm at average tip–substrate distances of z = 60 pm and z = 35 pm with respect to a tunneling current setpoint of I = 20 pA at U = 7 mV on Ag(111). The contrast of the Δf_2 images is very similar to conventional bond

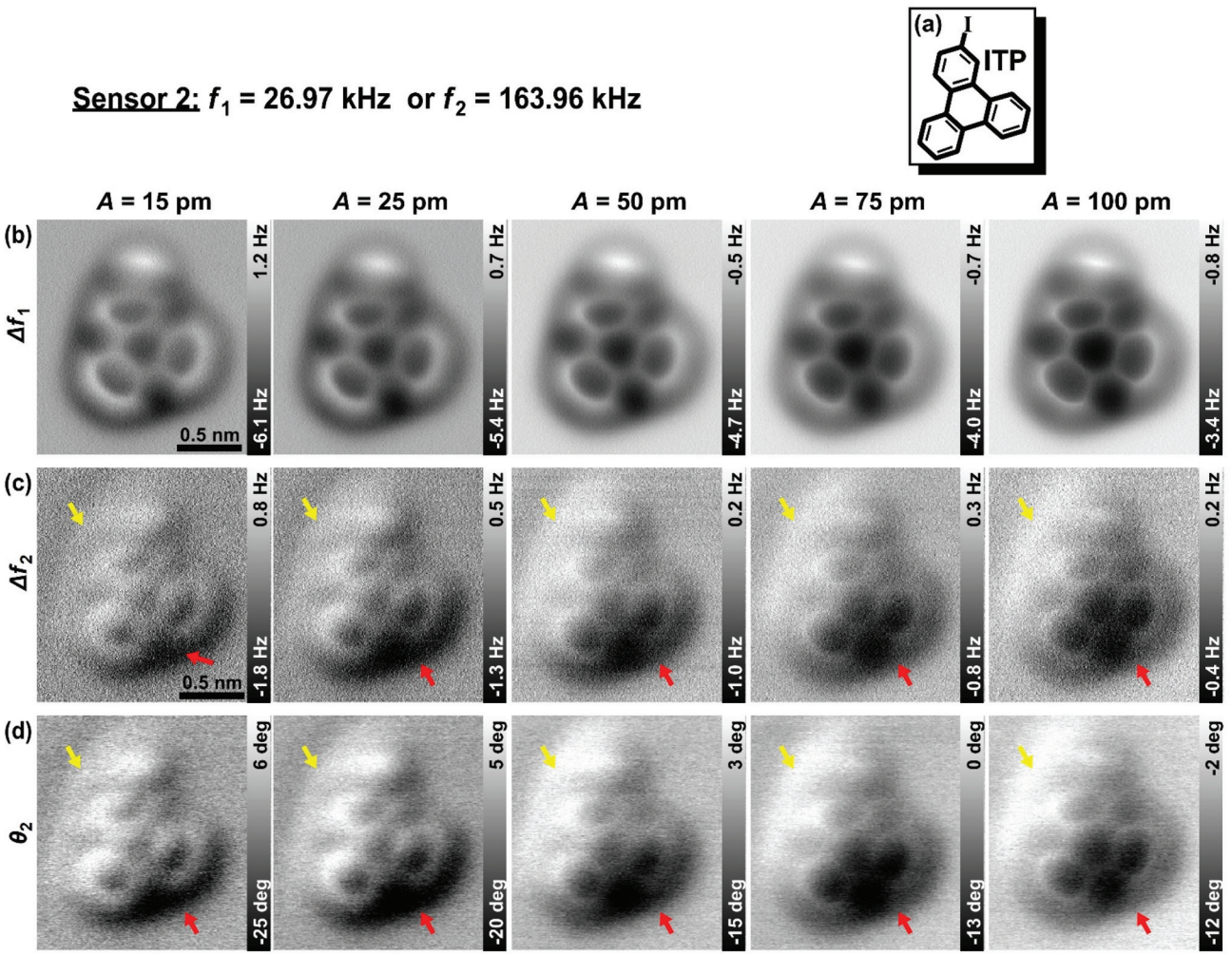

Fig. 3 (a) Chemical structure of ITP. Images of ITP on Cu(111) taken (b) by using the frequency shift (Δf_1) signal in FM mode with $f_1 \approx 26.97$ kHz, (c) frequency shift (Δf_2) signal in FM mode with $f_2 \approx 163.96$ kHz, and (d) the phase shift (θ_2) signal in AM mode with f_2 = 163.96 kHz. Images were taken with sensor 2 and oscillation amplitudes of 15, 25, 50, 75 and 100 pm. Scan speed: 333 pm s^{-1}.

images for the fundamental eigenmode. The C–C bonds appear as bright lines in the frequency shift images for relatively large tip–substrate distances (see Fig. 2f) and the contrast inverts when the tip is getting very close (Fig. 2g) (as reported in detail *e.g.* in ref. 25).

Next, we compared the image quality of the fundamental and 2nd flexural eigenmodes of sensor 2. Fig. 3b and 3c display constant height frequency shift images of 2-iodotriphenilene (ITP, see structure in Fig. 3a) on Cu(111) for both eigenmodes in a range of oscillation amplitudes from 15 to 100 pm. Apparently, the images at the 2nd flexural eigenmode reveal the same structural information of the imaged ITP molecules, however, their signal-to-noise performance is much lower compared to using the fundamental eigenmode. A direct comparison of single frequency shift scan lines above the molecules and the bare Ag(111) surface can be found in Fig. S2 in the ESI.† This comparison reveals almost the same absolute level of noise of the frequency shift signal of the fundamental and 2nd flexural eigenmode for all tested oscillation amplitudes (compare the blue curves in Fig. S2†). The absolute frequency shift values above the imaged molecule are, however, about one order of magnitude lower in the 2nd flexural mode, which leads to the lower image quality (compare the red curves in Fig. S2†).

The image quality of the 2nd flexural eigenmode can be significantly increased by operating the AFM in amplitude modulation (AM) mode (see Fig. 3d). It was recently reported that the signal-to-noise performance can be increased by approximately 30–60% by actuating the fundamental eigenmode in AM mode, which is related to the simpler electronics setup (without a phase-locked loop) and the slightly higher slope of the phase shift *vs.* distance curves.[63] In case of the fundamental eigenmode this usually requires a moderate reduction of the effective *Q*-factor *via* the Q-control method.[63–65] This is not needed in case of the 2nd flexural eigenmode due to the smaller absolute frequency shift values (which lead to minor changes of the oscillation amplitude during scanning).

In Fig. 4 we directly compare the image contrast and signal-to-noise performance of single line profiles that were obtained by exciting the fundamental eigenmode (in FM mode) and the 2nd flexural eigenmode (in FM and AM mode). The oscillation

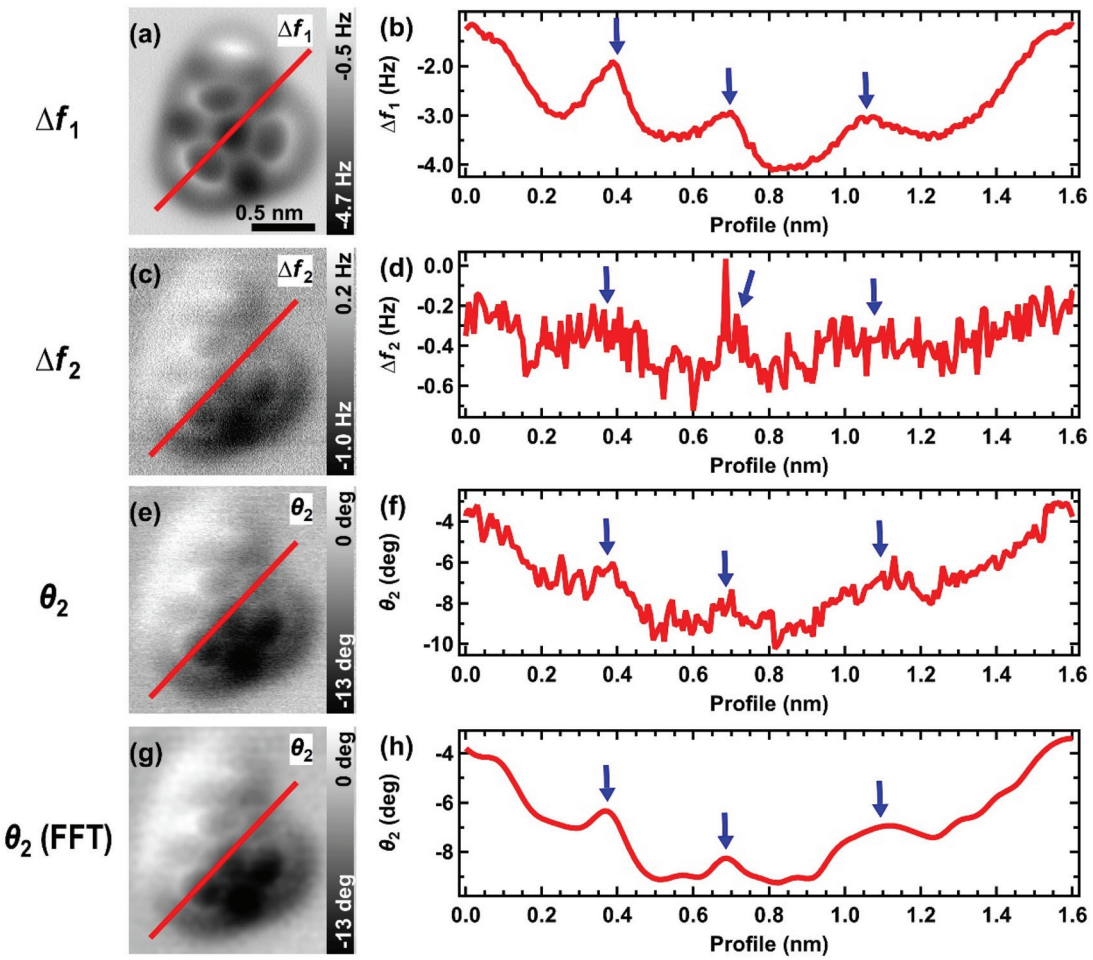

Fig. 4 (a–f) Images of ITP on Cu(111) and profiles along the molecule (as indicated by the red line in the AFM images) taken by sensor 2 (a and b) by using Δf_1 signal in FM mode, (c and d) Δf_2 signal in FM mode, and (e and f) θ_2 signal in AM mode (same images as in Fig. 3 for an oscillation amplitude of 50 pm). (g and h) Same image as in panel e after applying a 2D FFT filter and corresponding profile along the molecule.

amplitude was 50 pm in all cases. The line profiles for the 2nd flexural eigenmode (Fig. 4d and 4f) reveal a lower signal-to-noise performance for both operational modes. A significant advantage of AM mode over FM mode operation is revealed by these line profiles since the typical image features (see blue arrows) appear more clearly in the AM mode. In Fig. 4g and 4h we present filtered versions of the image and line profile in Fig. 4e and 4f. The image noise was removed by applying a 2D FFT filter[63] (see details in Fig. S3†). The structural features observed in filtered line profile in Fig. 4h (2nd flexural eigenmode, AM mode) and in the profile in Fig. 4a (fundamental eigenmode, FM mode) are in good agreement (see blue arrows).

A closer look at the 2nd flexural eigenmode images (Fig. 2f–g and 3c–d) reveals some asymmetric background features in the frequency shift (Δf_2) and phase (θ_2) signals across the scanned molecules. These appear as bright and dark features at the circumference of the imaged molecules, as highlighted by yellow and red arrows, respectively. The dashed blue lines in Fig. 2f–g indicate the axis of this background asymmetry. We conclude that these background features in the Δf_2 signal do not stem from the sample or the CO tip since they vanish when the qPlus sensor is actuated at the fundamental eigenmode (compare Fig. 3b and 3c, which were taken with the same CO-tip). Furthermore, these features appear for this qPlus sensor always at the same locations of the scanned molecules (please note that the images in Fig. 2f and 2g were scanned with a scanning angle of 0°, while 180° was used for Fig. 3).

These bright and dark features in the bond images are likely caused by an additional lateral component of the tip oscillation. Recently, we systematically analyzed the tip vibrations at the fundamental and higher eigenmodes of qPlus sensors using a laser Doppler vibrometer in ambient conditions.[57] Fig. 5 shows the measured mode shapes for a qPlus sensor whose geometry is similar to the sensors used in this

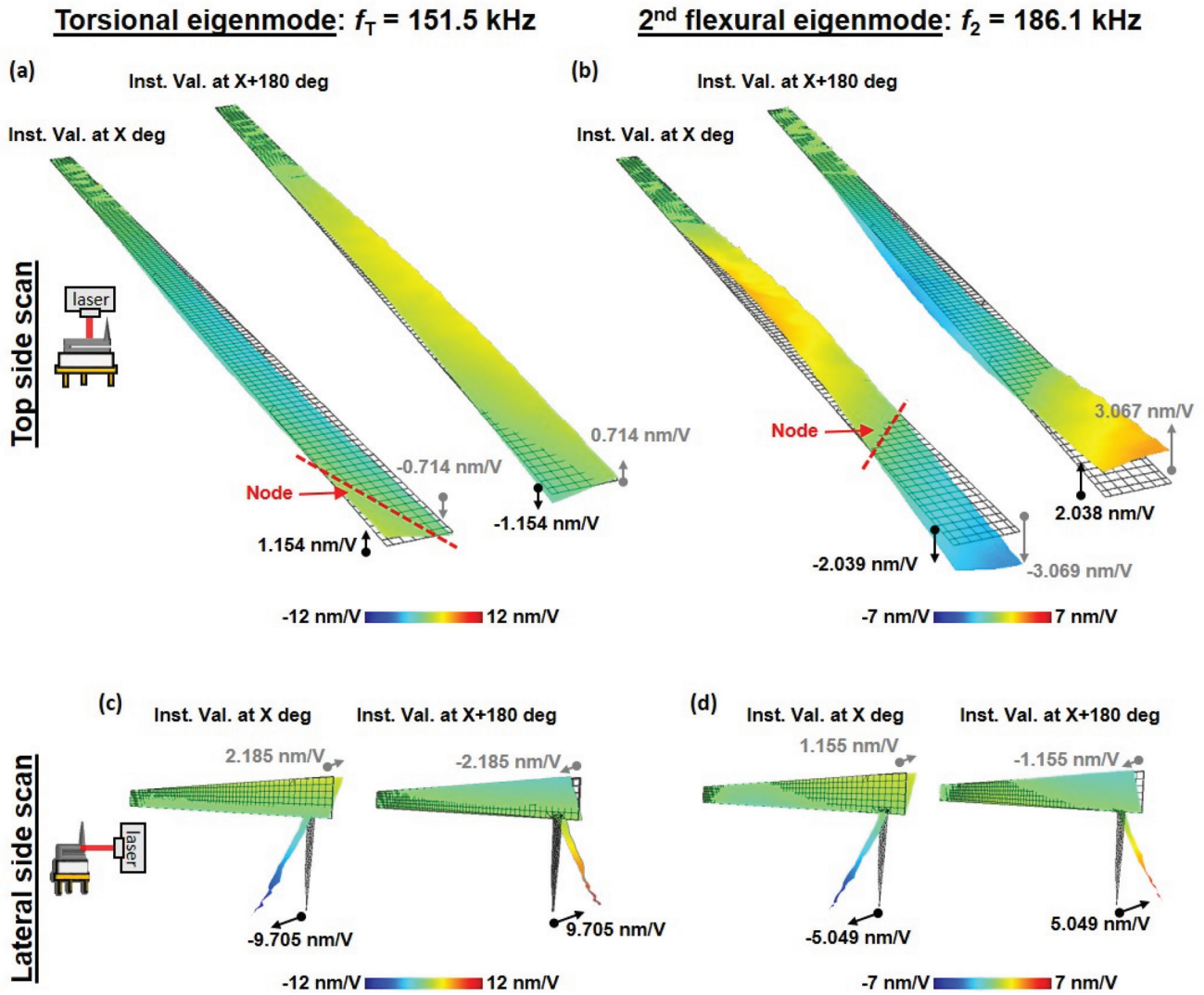

Fig. 5 (a–d) Eigenmode shapes of a qPlus sensor at the torsional and 2nd flexural eigenmode taken by laser Doppler vibrometer scans across the top and lateral side of the free prong. The panels a, b, c, d display the instantaneous sensitivities in nm V^{-1} at two oscillation positions, which are shifted by 180°.

study. For this sensor we found a torsional eigenmode at 151.5 kHz (Fig. 5a and 5c) and the 2nd flexural eigenmode at 186.1 kHz (Fig. 5b and 5d).

An analysis of torsional mode shape reveals that the tip moves almost exclusively in the lateral direction. The determined sensitivities at the location of the AFM tip (see black arrows) are approximately 1.2 nm V^{-1} for the vertical oscillation (Fig. 5a) and 9.7 nm V^{-1} for the lateral oscillation (Fig. 5c). Furthermore, the nodal line (dashed red line in Fig. 5a) is located at the end of the prong of the qPlus sensor, which indicates a low vertical movement at the torsional eigenmode.

For the 2nd flexural eigenmode, however, the node (dashed red line in Fig. 5b) is not located at the very end of the prong and not perpendicular to the long axis of the prong, leading to simultaneous vertical and lateral oscillations. The vertical and lateral oscillation sensitivities are 2.0 nm V^{-1} and 5.0 nm V^{-1}, respectively (black arrows in Fig. 5b and 5d). Hence, for this sensor, the amount of lateral *vs.* vertical oscillation at the 2nd flexural eigenmode is on the order of 250% resulting in a diagonal movement of the tip. Please note that this behavior of the 2nd flexural eigenmode depends strongly on the size and position of the tungsten wire at the end of the prong of the qPlus sensor. For other qPlus sensors with different tip geometries, we measured lateral movements ranging from 80% to 175% *via* laser Doppler vibrometry.[57] Hence, it is likely that the sensor 2 we used for the bond imaging experiments also oscillates diagonally at its 2nd flexural eigenmode, although it is difficult to estimate its precise lateral movement without performing laser Doppler vibrometry measurements for exactly this sensor.

For analyzing the effect of such a diagonal tip movement (superposition of in phase vertical and lateral movements) on the submolecular image contrast, we performed AFM simulations with the so-called probe particle model.[58] This simulation method is frequently used in the literature and has shown that it can adequately reproduce the basic features of bond images.[66–70] As illustrated in Fig. S4,† the vertical movement of a tilted CO-tip is similar to a diagonal movement of a straight CO-tip. Since the original probe particle model as published by Hapala *et al.*[58] already provides an input parameter for adjusting the tilt of the CO tip, we simply simulated AFM images of adsorbed ITP molecules for tilted and non-tilted tip geometries to compare these with our experimental AFM images.

Fig. 6a and 6b show an experimental AFM image and a line profile of ITP on Cu(111) that were obtained with sensor 2 at its fundamental eigenmode (same images as in Fig. 3 for an oscillation amplitude of 100 pm). Fig. 6d and 6e show a corresponding simulated AFM image and line profile that were obtained with a non-tilted vertically oscillating CO-tip. In view of the simplicity of the applied probe particle method the agreement between the experimental and simulated line profiles is remarkable. In particular, the subtle difference in brightnesses of the three C–C bonds which are crossed by the line profile (dashed red line) are reproduced by the simulation (see the three blue arrows in Fig. 6b and 6e).

In case of the 2nd flexural eigenmode, these differences in brightness are much more pronounced, *i.e.* at the left side of the scan line in Fig. 6g, the C–C bonds appear much brighter than at the right side (see blue arrows). It looks as if the ITP molecule assumes a tilted adsorption conformation, which is obviously not the case as confirmed by the images and scanlines of the fundamental eigenmode (Fig. 6a and 6b). The apparent tilt in the scanline in Fig. 6g can be reproduced by the AFM simulation if a tilted CO-tip is considered (compare

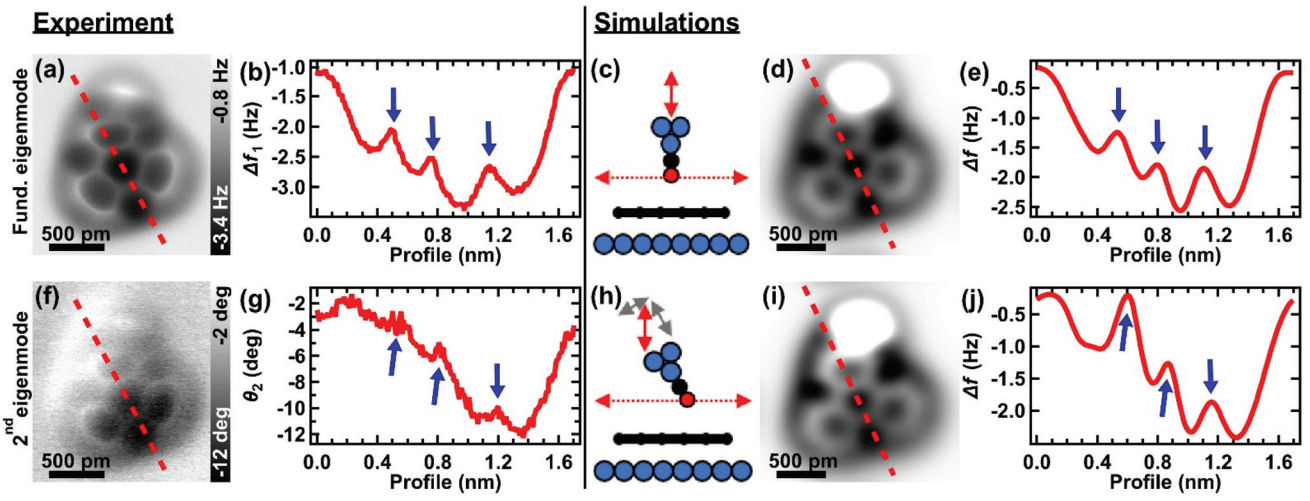

Fig. 6 (a) Δf_1 images of ITP on Cu(111) with A = 100 pm taken with sensor 2. (b) Profile along the dashed red line in image a. (c) Scheme depicting the setup for the AFM simulation with the probe particle model: A non-tilted tip oscillates vertically above the substrate. (d) Simulated AFM image of ITP for a straight tip. (e) Profile along the dashed red line in image d. (f) θ_2 images of ITP on Cu(111) with A = 100 pm taken with sensor 2. (g) Profile along the dashed red line in image f. (h) Here a tilted tip (16° *vs.* z-axis) that oscillates vertically was considered for the probe-particle-model simulation. (i) Simulated AFM image of ITP for a tilted tip. (j) Profile along the dashed red line in image i.

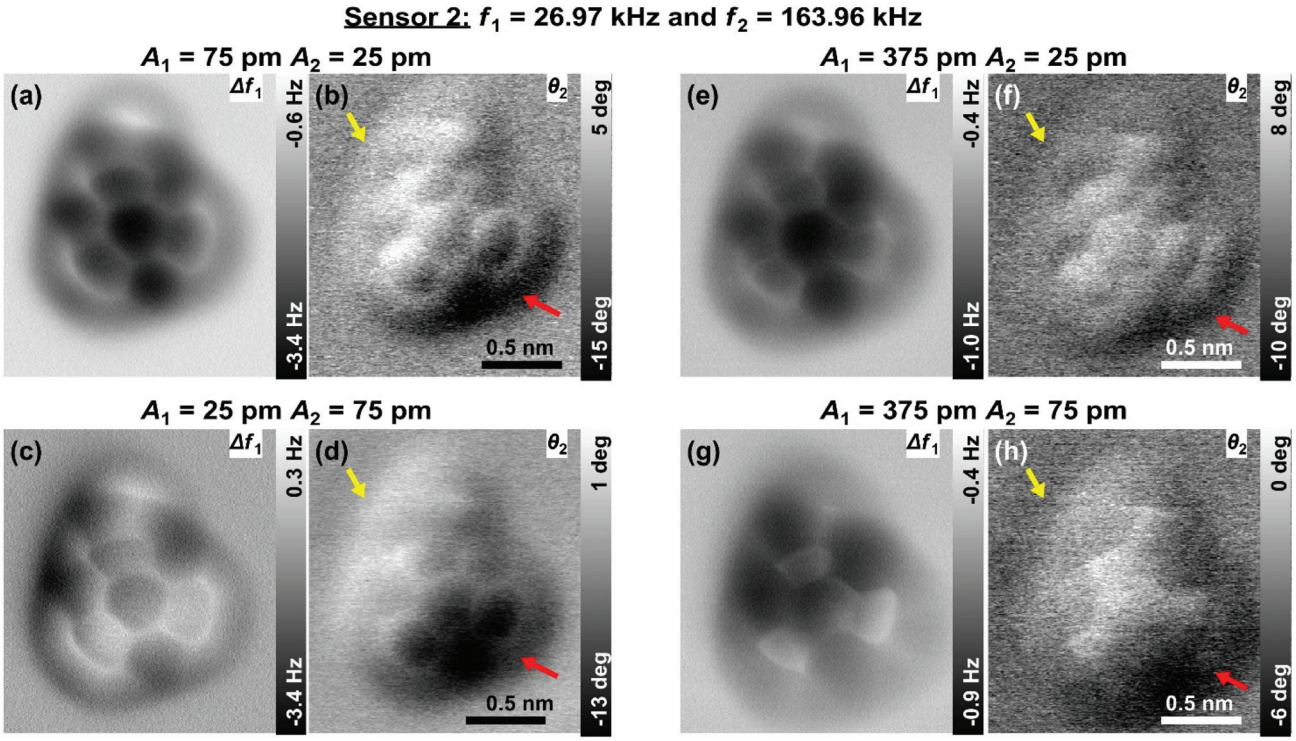

Fig. 7 (a–h) Bimodal FM_1–AM_2 (Δf_1 and θ_2) images of ITP on Cu(111) at constant height with (a, b) A_1 = 75 pm, A_2 = 25 pm, (c, d) A_1 = 25 pm, A_2 = 75 pm, (e, f) A_1 = 375 pm, A_2 = 25 pm and (g, h) A_1 = 375 pm, A_2 = 75 pm. Scan speed: 333 pm s^{-1}.

blue arrows in Fig. 6g and 6j). As a tilted tip has a similar effect as a diagonal tip oscillation (see illustration in Fig. S4†) we can rationalize that this observed apparent tilting of the ITP is an image artifact caused by the diagonal tip movement at the 2nd flexural eigenmode of the qPlus sensor.

3.3 Bimodal AFM

Finally, we used qPlus sensor 2 to perform bimodal bond imaging AFM by simultaneously exciting its fundamental and its 2nd flexural eigenmode. The fundamental mode was operated in FM mode while the AM mode was used for the 2nd flexural mode. Fig. 7 shows images for four different combinations of oscillation amplitudes. In case of relatively small amplitudes (Fig. 7a–d) the bimodal images look rather similar to the corresponding images for single mode excitation (*cf.* Fig. 3). However, a detailed look at the images of the fundamental eigenmode (Fig. 7a and c) reveals some slight distortions that are presumably caused by the lateral component of the 2nd flexural eigenmode. For larger amplitudes of the fundamental mode (Fig. 7e and 7g) these distortions become more severe. In that case, the images of the 2nd flexural mode (Fig. 7f and 7h) are heavily distorted.

Conclusions

We systematically analyzed the bond imaging performance of qPlus sensors when using torsional and flexural higher eigenmodes. In particular, the torsional eigenmode of qPlus sensor 1 seems perfectly suited to perform LFM with single bond resolution. As in previous studies, we found that the tip oscillates almost exclusively in the lateral direction at the torsional mode.[57] This is very promising for future studies, since it enables an easy switching between vertical and lateral bond imaging without changing qPlus sensors. The image quality at the torsional eigenmode is comparable to that of customized qPlus sensors specifically designed for LFM operation. When using the 2nd flexural eigenmode of qPlus sensor 2 we observed a lower image quality as well as dark and bright image features and an apparent tilting of the molecules. The lower signal-to-noise performance could be somewhat improved by applying the AM mode instead of the FM mode, however, it was not as high as for the fundamental eigenmode. The additional dark and bright image features were assigned to diagonal oscillations of the tip. These results are useful for designing new qPlus sensors in the future. The lateral component of the tip oscillation may, for example, be significantly reduced by using smaller tips and adjusting their position at the end of the prong of the qPlus sensor. Furthermore, by customizing the layout of the electrodes of the qPlus sensors it should be possible to improve the signal quality at the 2nd flexural eigenmode. In general, we see a very high potential for future applications of multifrequency AFM techniques in the case of qPlus sensors. Since chemical bond resolution is already observed in case of our conventional non-optimized qPlus sensors, we believe that with the mentioned tweaks one

could achieve comparable or even increased signal-to-noise performance at higher eigenmodes.

Conflicts of interest

There are no conflicts to declare.

Acknowledgements

M. G. Ruppert and D. Ebeling wish to acknowledge the funding support from the German Research Foundation (Deutsche Forschungsgemeinschaft, DFG) under the category 'Initiation of International Collaborations' with reference EB 535/2-1. Further funding was provided by the Deutsche Forschungsgemeinschaft *via* grants EB 535/1-1 (D.E.), SCHI 619/13 (A.S.) and the GRK (Research Training Group) 2204 'Substitute Materials for Sustainable Energy Technologies' (A. S.). We also gratefully acknowledge financial support by the LOEWE Program of Excellence of the Federal State of Hesse (LOEWE Focus Group PriOSS 'Principles of On-Surface Synthesis' (A.S.).

Notes and references

1 G. Binnig, C. F. Quate and C. Gerber, Atomic force microscope, *Phys. Rev. Lett.*, 1986, **56**, 930.
2 F. J. Giessibl, Advances in atomic force microscopy, *Rev. Mod. Phys.*, 2003, **75**, 949.
3 S. M. R. Akrami, H. Nakayachi, T. Watanabe-Nakayama, H. Asakawa and T. Fukuma, Significant improvements in stability and reproducibility of atomic-scale atomic force microscopy in liquid, *Nanotechnology*, 2014, **25**, 455701.
4 Y. F. Dufrêne, T. Ando, R. Garcia, D. Alsteens, D. Martinez-Martin, A. Engel, C. Gerber and D. J. Müller, Imaging modes of atomic force microscopy for application in molecular and cell biology, *Nat. Nanotechnol.*, 2017, **12**, 295–307.
5 D. J. Müller, A. C. Dumitru, C. Lo Giudice, H. E. Gaub, P. Hinterdorfer, G. Hummer, J. J. de Yoreo, Y. F. Dufrêne and D. Alsteens, Atomic force microscopy-based force spectroscopy and multiparametric imaging of biomolecular and cellular systems, *Chem. Rev.*, 2021, **121**, 11701–11725.
6 S. Santos, K. Gadelrab, C. Y. Lai, T. Olukan, J. Font, V. Barcons, A. Verdaguer and M. Chiesa, Advances in dynamic AFM: From nanoscale energy dissipation to material properties in the nanoscale, *J. Appl. Phys.*, 2021, **129**, 134302.
7 L. Gross, F. Mohn, N. Moll, P. Liljeroth and G. Meyer, The chemical structure of a molecule resolved by atomic force microscopy, *Science*, 2009, **325**, 1110–1114.
8 D. G. de Oteyza, P. Gorman, Y. C. Chen, S. Wickenburg, A. Riss, D. J. Mowbray, G. Etkin, Z. Pedramrazi, H.-Z. Tsai, A. Rubio, M. F. Crommie and F. R. Fischer, Direct imaging of covalent bond structure in single-molecule chemical reactions, *Science*, 2013, **340**, 1434–1437.
9 F. Albrecht, M. Neu, C. Quest, I. Swart and J. Repp, Formation and characterization of a molecule–metal–molecule bridge in real space, *J. Am. Chem. Soc.*, 2013, **135**, 9200–9203.
10 A. Riss, A. P. Paz, S. Wickenburg, H. Z. Tsai, D. G. de Oteyza, A. J. Bradley, M. M. Ugeda, P. Gorman, H. S. Jung, M. F. Crommie, A. Rubio and F. R. Fischer, Imaging single-molecule reaction intermediates stabilized by surface dissipation and entropy, *Nat. Chem.*, 2016, **8**, 678–683.
11 S. Kawai, A. Sadeghi, T. Okamoto, C. Mitsui, R. Pawlak, T. Meier, J. Takeya, S. Goedecker and E. Meyer, Organometallic Bonding in an Ullmann–Type On–Surface Chemical Reaction Studied by High–Resolution Atomic Force Microscopy, *Small*, 2016, **12**, 5303–5311.
12 S. Zint, D. Ebeling, T. Schlöder, S. Ahles, D. Mollenhauer, H. A. Wegner and A. Schirmeisen, Imaging successive intermediate states of the on-surface Ullmann reaction on Cu (111): role of the metal coordination, *ACS Nano*, 2017, **11**, 4183–4190.
13 C. Steiner, J. Gebhardt, M. Ammon, Z. Yang, A. Heidenreich, N. Hammer, A. Görling, M. Kivala and S. Maier, Hierarchical on-surface synthesis and electronic structure of carbonyl-functionalized one-and two-dimensional covalent nanoarchitectures, *Nat. Commun.*, 2017, **8**, 1–11.
14 Q. Fan, D. Martin-Jimenez, D. Ebeling, C. K. Krug, L. Brechmann, C. Kohlmeyer, G. Hilt, W. Hierunger, A. Schirmeisen and J. M. Gottfried, Nanoribbons with non-alternant topology from fusion of polyazulene: Carbon allotropes beyond graphene, *J. Am. Chem. Soc.*, 2019, **141**, 17713–17720.
15 X. Zhang, N. Xue, C. Li, N. Li, H. Wang, N. Kocić, S. Beniwal, K. Palotás, R. Li, Q. Xue, S. Maier, S. Hou and Y. Wang, Coordination-controlled C–C coupling products via ortho-site C–H activation, *ACS Nano*, 2019, **13**, 1385–1393.
16 Q. Fan, D. Martin-Jimenez, S. Werner, D. Ebeling, T. Koehler, T. Vollgraff, J. Sundermeyer, W. Hierunger, A. Schirmeisen and J. M. Gottfried, On-surface synthesis and characterization of a cycloarene: C108 graphene ring, *J. Am. Chem. Soc.*, 2020, **142**, 894–899.
17 A. Ishii, A. Shiotari and Y. Sugimoto, Quality control of on-surface-synthesised seven-atom wide armchair graphene nanoribbons, *Nanoscale*, 2020, **12**, 6651–6657.
18 L. Liu, H. Klaasen, M. C. Witteler, B. Schulze Lammers, B. A. Timmer, H. Kong, H. Mönig, H.-Y. Gao, J. Neugebauer, H. Fuchs and A. Studer, Polymerization of silanes through dehydrogenative Si–Si bond formation on metal surfaces, *Nat. Chem.*, 2021, **13**, 350–357.
19 Q. Zhong, A. Ihle, S. Ahles, H. A. Wegner, A. Schirmeisen and D. Ebeling, Constructing covalent organic nanoarchitectures molecule by molecule via scanning probe manipulation, *Nat. Chem.*, 2021, **13**, 1133–1139.
20 S. Clair and D. G. de Oteyza, Controlling a chemical coupling reaction on a surface: tools and strategies for on-surface synthesis, *Chem. Rev.*, 2019, **119**, 4717–4776.

21 L. Grill and S. Hecht, Covalent on-surface polymerization, *Nat. Chem.*, 2020, **12**, 115–130.
22 F. J. Giessibl, Atomic resolution on Si (111)-(7 × 7) by non-contact atomic force microscopy with a force sensor based on a quartz tuning fork, *Appl. Phys. Lett.*, 2000, **76**, 1470–1472.
23 L. Bartels, G. Meyer and K. H. Rieder, Controlled vertical manipulation of single CO molecules with the scanning tunneling microscope: A route to chemical contrast, *Appl. Phys. Lett.*, 1997, **71**, 213–215.
24 B. Schulze Lammers, D. Yesilpinar, A. Timmer, Z. Hu, W. Ji, S. Amirjalayer, H. Fuchs and H. Mönig, Benchmarking atomically defined AFM tips for chemical-selective imaging, *Nanoscale*, 2021, **13**, 13617–13623.
25 D. Martin-Jimenez, S. Ahles, D. Mollenhauer, H. A. Wegner, A. Schirmeisen and D. Ebeling, Bond-level imaging of the 3D conformation of adsorbed organic molecules using atomic force microscopy with simultaneous tunneling feedback, *Phys. Rev. Lett.*, 2019, **122**, 196101.
26 T. R. Albrecht, P. Grütter, D. Horne and D. Rugar, Frequency modulation detection using high–Q cantilevers for enhanced force microscope sensitivity, *J. Appl. Phys.*, 1991, **69**, 668–673.
27 F. J. Giessibl, The qPlus sensor, a powerful core for the atomic force microscope, *Rev. Sci. Instrum.*, 2019, **90**, 011101.
28 S. Kawai, S. I. Kitamura, D. Kobayashi and H. Kawakatsu, Dynamic lateral force microscopy with true atomic resolution, *Appl. Phys. Lett.*, 2005, **87**, 173105.
29 O. Sahin, S. Magonov, C. Su, C. F. Quate and O. Solgaard, An atomic force microscope tip designed to measure time-varying nanomechanical forces, *Nat. Nanotechnol.*, 2007, **2**, 507–514.
30 R. W. Stark, Dynamics of repulsive dual-frequency atomic force microscopy, *Appl. Phys. Lett.*, 2009, **94**, 063109.
31 Y. J. Li, K. Takahashi, N. Kobayashi, Y. Naitoh, M. Kageshima and Y. Sugawara, Multifrequency high-speed phase-modulation atomic force microscopy in liquids, *Ultramicroscopy*, 2010, **110**, 582–585.
32 S. Kawai, T. Glatzel, S. Koch, B. Such, A. Baratoff and E. Meyer, Ultrasensitive detection of lateral atomic-scale interactions on graphite (0001) via bimodal dynamic force measurements, *Phys. Rev. B*, 2010, **81**, 085420.
33 R. Garcia and E. T. Herruzo, The emergence of multifrequency force microscopy, *Nat. Nanotechnol.*, 2012, **7**, 217.
34 S. Guo, S. D. Solares, V. Mochalin, I. Neitzel, Y. Gogotsi, S. V. Kalinin and S. Jesse, Multifrequency imaging in the intermittent contact mode of atomic force microscopy: beyond phase imaging, *Small*, 2012, **8**, 1264–1269.
35 D. Kiracofe, A. Raman and D. Yablon, Multiple regimes of operation in bimodal AFM: understanding the energy of cantilever eigenmodes, *Beilstein J. Nanotechnol.*, 2013, **4**, 385–393.
36 S. S. Borysov, D. Platz, A. S. de Wijn, D. Forchheimer, E. A. Tolén, A. V. Balatsky and D. B. Haviland, Reconstruction of tip-surface interactions with multimodal intermodulation atomic force microscopy, *Phys. Rev. B*, 2013, **88**, 115405.
37 D. Ebeling, B. Eslami and S. D. J. Solares, Visualizing the subsurface of soft matter: simultaneous topographical imaging, depth modulation, and compositional mapping with triple frequency atomic force microscopy, *ACS Nano*, 2013, **7**, 10387–10396.
38 D. Ebeling and S. D. Solares, Amplitude modulation dynamic force microscopy imaging in liquids with atomic resolution: comparison of phase contrasts in single and dual mode operation, *Nanotechnology*, 2013, **24**, 135702.
39 E. T. Herruzo, A. P. Perrino and R. Garcia, Fast nanomechanical spectroscopy of soft matter, *Nat. Commun.*, 2014, **5**, 1–8.
40 C. Moreno, O. Stetsovych, T. K. Shimizu and O. Custance, Imaging three-dimensional surface objects with submolecular resolution by atomic force microscopy, *Nano Lett.*, 2015, **15**, 2257–2262.
41 M. Damircheli, A. F. Payam and R. Garcia, Optimization of phase contrast in bimodal amplitude modulation AFM, *Beilstein J. Nanotechnol.*, 2015, **6**, 1072–1081.
42 C. Y. Lai, S. Santos and M. Chiesa, Systematic multidimensional quantification of nanoscale systems from bimodal atomic force microscopy data, *ACS Nano*, 2016, **10**, 6265–6272.
43 C. A. Amo, A. P. Perrino, A. F. Payam and R. Garcia, Mapping elastic properties of heterogeneous materials in liquid with angstrom-scale resolution, *ACS Nano*, 2017, **11**, 8650–8659.
44 A. J. Weymouth, Non-contact lateral force microscopy, *J. Phys.: Condens. Matter*, 2017, **29**, 323001.
45 V. G. Gisbert, C. A. Amo, M. Jaafar, A. Asenjo and R. Garcia, Quantitative mapping of magnetic properties at the nanoscale with bimodal AFM, *Nanoscale*, 2021, **13**, 2026–2033.
46 B. Rajabifar, A. Bajaj, R. Reifenberger, R. Proksch and A. Raman, Discrimination of adhesion and viscoelasticity from nanoscale maps of polymer surfaces using bimodal atomic force microscopy, *Nanoscale*, 2021, **13**, 17428–17441.
47 A. L. Eichhorn and C. Dietz, Simultaneous Deconvolution of In–Plane and Out–of–Plane Forces of HOPG at the Atomic Scale under Ambient Conditions by Multifrequency Atomic Force Microscopy, *Adv. Mater. Interfaces*, 2021, **8**, 2101288.
48 A. Bettac, J. Koeble, K. Winkler, B. Uder, M. Maier and A. Feltz, QPlus: atomic force microscopy on single-crystal insulators with small oscillation amplitudes at 5 K, *Nanotechnology*, 2009, **20**, 264009.
49 R. C. Tung, T. Wutscher, D. Martinez-Martin, R. G. Reifenberger, F. Giessibl and A. Raman, Higher-order eigenmodes of qPlus sensors for high resolution dynamic atomic force microscopy, *J. Appl. Phys.*, 2010, **107**, 104508.
50 H. Ooe, D. Kirpal, D. S. Wastl, A. J. Weymouth, T. Arai and F. J. Giessibl, Amplitude dependence of image quality in atomically-resolved bimodal atomic force microscopy, *Appl. Phys. Lett.*, 2016, **109**, 141603.

51 D. Ebeling, Q. Zhong, S. Ahles, L. Chi, H. A. Wegner and A. Schirmeisen, Chemical bond imaging using higher eigenmodes of tuning fork sensors in atomic force microscopy, *Appl. Phys. Lett.*, 2017, **110**, 183102.
52 B. Kim, J. Jahng, R. M. Khan, S. Park and E. O. Potma, Eigenmodes of a quartz tuning fork and their application to photoinduced force microscopy, *Phys. Rev. B*, 2017, **95**, 075440.
53 Y. Yamada, T. Ichii, T. Utsunomiya and H. Sugimura, Simultaneous detection of vertical and lateral forces by bimodal AFM utilizing a quartz tuning fork sensor with a long tip, *Jpn. J. Appl. Phys.*, 2019, **58**, 095003.
54 D. Kirpal, J. Qiu, K. Pürckhauer, A. J. Weymouth, M. Metz and F. J. Giessibl, Biaxial atomically resolved force microscopy based on a qPlus sensor operated simultaneously in the first flexural and length extensional modes, *Rev. Sci. Instrum.*, 2021, **92**, 043703.
55 A. J. Weymouth, E. Riegel, O. Gretz and F. J. Giessibl, Strumming a single chemical bond, *Phys. Rev. Lett.*, 2020, **124**, 196101.
56 A. J. Weymouth, E. Riegel, B. Simmet, O. Gretz and F. J. Giessibl, Lateral Force Microscopy Reveals the Energy Barrier of a Molecular Switch, *ACS Nano*, 2021, **15**, 3264–3271.
57 M. G. Ruppert, D. Martin-Jimenez, Y. K. Yong, A. Ihle, A. Schirmeisen, A. J. Fleming and D. Ebeling, Experimental Analysis of Tip Vibrations at Higher Eigenmodes of QPlus Sensors for Atomic Force Microscopy, *Nanotechnology*, 2022, **33**, 185503.
58 P. Hapala, G. Kichin, C. Wagner, F. S. Tautz, R. Temirov and P. Jelínek, Mechanism of high-resolution STM/AFM imaging with functionalized tips, *Phys. Rev. B: Condens. Matter Mater. Phys.*, 2014, **90**, 085421.
59 G. H. Simon, M. Heyde and H. P. Rust, Recipes for cantilever parameter determination in dynamic force spectroscopy: spring constant and amplitude, *Nanotechnology*, 2007, **18**, 255503.
60 S. Zint, D. Ebeling, S. Ahles, H. A. Wegner and A. Schirmeisen, Subsurface-controlled angular rotation: triphenylene molecules on Au (111) substrates, *J. Phys. Chem. C*, 2016, **120**, 1615–1622.
61 M. G. Ruppert, S. I. Moore, M. Zawierta, A. J. Fleming, G. Putrino and Y. K. Yong, Multimodal atomic force microscopy with optimized higher eigenmode sensitivity using on-chip piezoelectric actuation and sensing, *Nanotechnology*, 2019, **30**, 085503.
62 O. Pfeiffer, R. Bennewitz, A. Baratoff, E. Meyer and P. Grütter, Lateral-force measurements in dynamic force microscopy, *Phys. Rev. B*, 2002, **65**, 161403.
63 D. Martin-Jimenez, A. Ihle, S. Ahles, H. A. Wegner, A. Schirmeisen and D. Ebeling, Bond-level imaging of organic molecules using Q-controlled amplitude modulation atomic force microscopy, *Appl. Phys. Lett.*, 2020, **117**, 131601.
64 H. Hölscher, D. Ebeling and U. D. Schwarz, Theory of Q-controlled dynamic force microscopy in air, *J. Appl. Phys.*, 2006, **99**, 084311.
65 O. E. Dagdeviren, J. Götzen, H. Hölscher, E. I. Altman and U. D. Schwarz, Robust high-resolution imaging and quantitative force measurement with tuned-oscillator atomic force microscopy, *Nanotechnology*, 2016, **27**, 065703.
66 P. Hapala, M. Švec, O. Stetsovych, N. J. van der Heijden, M. Ondráček, J. van der Lit, P. Mutombo, I. Swart and P. Jelínek, Mapping the electrostatic force field of single molecules from high-resolution scanning probe images, *Nat. Commun.*, 2016, **7**, 1–8.
67 F. Schulz, J. Ritala, O. Krejci, A. P. Seitsonen, A. S. Foster and P. Liljeroth, Elemental identification by combining atomic force microscopy and kelvin probe force microscopy, *ACS Nano*, 2018, **12**, 5274–5283.
68 J. Peng, J. Guo, P. Hapala, D. Cao, R. Ma, B. Cheng, L. Xu, M. Ondráček, P. Jelínek, E. Wang and Y. Jiang, Weakly perturbative imaging of interfacial water with submolecular resolution by atomic force microscopy, *Nat. Commun.*, 2018, **9**, 1–7.
69 Q. Zhong, Y. Hu, K. Niu, H. Zhang, B. Yang, D. Ebeling, J. Tschakert, T. Cheng, A. Schirmeisen, A. Narita, K. Müllen and L. Chi, Benzo-fused periacenes or double helicenes? Different cyclodehydrogenation pathways on surface and in solution, *J. Am. Chem. Soc.*, 2019, **141**, 7399–7406.
70 B. Alldritt, P. Hapala, N. Oinonen, F. Urtev, O. Krejci, F. F. Canova, J. Kannala, F. Schulz, P. Liljeroth and A. S. Foster, Automated structure discovery in atomic force microscopy, *Sci. Adv.*, 2020, **6**, eaay6913.